

Atmospheric complexity or scale by scale simplicity?

S. Lovejoy,¹ D. Schertzer,^{2,3} V. Allaire,¹ T. Bourgeois,² S. King,¹ J. Pinel,¹ and J. Stolle¹

Received 30 August 2008; revised 6 November 2008; accepted 10 November 2008; published 1 January 2009.

[1] Is the numerical integration of nonlinear partial differential equations the only way to tackle atmospheric complexity? Or do cascade dynamics repeating scale after scale lead to simplicity? Using 1000 orbits of TRMM satellite radiances from 11 bands in the short wave (visible, infra red) long wave (passive microwave) and radar regions and 8.8 to 20,000 km in scale, we find that the radiance gradients follow the predictions of cascade theories to within about $\pm 0.5\%$, $\pm 1.25\%$, $\pm 5.9\%$ for the short waves, long waves and reflectivities respectively and with outer scales varying between $\approx 5,000$ to $\approx 32,000$ km. Since the radiances and dynamics are strongly coupled, we conclude that weather can be accurately modeled as a cascade process. **Citation:** Lovejoy, S., D. Schertzer, V. Allaire, T. Bourgeois, S. King, J. Pinel, and J. Stolle (2009), Atmospheric complexity or scale by scale simplicity?, *Geophys. Res. Lett.*, *36*, L01801, doi:10.1029/2008GL035863.

1. Introduction

[2] In 1922, Lewis Fry Richardson published the now celebrated book “Weather forecasting by numerical process” [Richardson, 1922] in which he daringly proposed that the weather could be forecast by brute force numerical integration of coupled nonlinear partial differential equations (PDE’s). But the father of numerical weather prediction was Janus-faced: his book contains a famous phrase in which he proposed that the complex nonlinear atmospheric dynamics cascaded scale after scale from planetary down to small viscous scales. Shortly afterwards [Richardson, 1926], he suggested that atmospheric particle trajectories might be Wierstrasse-like functions (fractals) with simple (but non-classical) scale by scale regularity. Richardson apparently believed that messy complexity ought to give way to scale by scale simplicity: he is often considered the grandfather of modern cascade models.

[3] Today, numerical forecasting is a daily reality; but what about the dream of scale by scale simplicity embodied in cascades? For a long time after Richardson, cascades were inspirational and were regularly invoked in turbulence theories. However, it was not until the development of explicit multiplicative cascade models (starting in the 1960’s and 70’s [e.g., Novikov and Stewart, 1964; Yaglom, 1966; Mandelbrot, 1974]) that empirically verifiable cascade predictions could go much beyond the determination of (non intermittent) spectral exponents and of the up scale or down

scale cascade direction [see, e.g., Boer and Shepherd, 1983; Chen and Wiin-Nielsen, 1978; Strauss and Ditlevsen, 1999].

[4] By the 1980’s it was realized that multiplicative cascade models were the generic multifractal process. Subsequent developments have shown their great generality which have spawned applications throughout physics and the geosciences. In particular, while today there is a general consensus that at least over some scale range the atmosphere is multifractal, there have not yet been planetary scale investigations of the precise predictions of these explicit cascade models (equation 1 below). One of the reasons is that the dynamically most important fields must be measured in situ and this introduces numerous difficulties of interpretation (e.g., both (sparse) networks and aircraft trajectories can themselves be fractal [Lovejoy et al., 1986, 2004; S. Lovejoy et al., Reinterpreting aircraft measurements in anisotropic scaling turbulence, submitted to *Atmospheric Physics and Chemistry*, 2008] and sonde outages can be multifractal (S. Lovejoy et al., The vertical cascade structure of the atmosphere and multifractal drop sonde outages, *Journal of Geophysical Research*, in press, 2008)). Consequently it is advantageous to use remotely sensed radiances: the largest relevant study [Lovejoy et al., 2001] used nearly one thousand 256×256 pixel “scenes” of satellite visible and Infra red radiances over the range 2.2 to 280 km. While the fields accurately displayed cascade statistics, the largest scales - including the key outer scale of the variability - was only indirectly estimated by extrapolation well beyond the measured range. Up until now, these shortcomings have made it possible to dismiss the idea that scaling might hold up to near planetary scales or over wide ranges and to continue to pursue approaches incompatible with scaling.

[5] Although the study [Lovejoy et al., 2001] had a hundred times the data content of the largest in situ turbulence experiment - it was small by today’s standards. In this paper, we use about one thousand orbits of visible, infra red (IR), passive and active microwave data (11 bands in all) from the Tropical Rainfall Monitoring Mission (TRMM) satellite to directly extend these analyses to 20,000 km. Because of this wide range and the fact that each orbit comprises about the same amount of data as the entire previous study, this paper provides the first near “empirical proof” of wide range, planetary scale cascade scaling.

2. Data

[6] We analyze data from the Visible and Infrared Scanner (VIRS) [Barnes et al., 1999], the Thermal Microwave Imager (TMI) [Kummerow et al., 1997] and the precipitation radar (PR) (TRMM Precipitation radar team, 2005) from the TRMM satellite (launched on November 27,

¹Physics, McGill University, Montreal, Quebec, Canada.

²CEREVE, Université Paris Est, Mame-la Vallée France.

³Also at Météo France, Paris, France.

Table 1. Characteristics of the Five Visible and Infra Red Bands

Band	Wavelength	Resolution (km)	$\bar{\delta}$ (%)	C_1	L_{eff} (km)
VIRS 1	0.630 μm	8.8	0.53	0.077	13800
VIRS 2	1.60 μm	8.8	0.61	0.079	25000
VIRS 3	3.75 μm	22.	0.35	0.065	28200
VIRS 4	10.8 μm	8.8	0.37	0.081	11200
VIRS 5	12.2 μm	8.8	0.36	0.084	12600

1997, in an orbit between $\pm 38^\circ$ latitude at 350 km altitude, period of 91 minutes). VIRS has five separate bands, ranging from the visible to thermal infrared (Table 1). The nominal resolutions were 2.2 km, with a 720 km swath width. TMI has nine microwave bands (four of which are dual polarization) with swath width 760 km (Table 2). The nominal resolution at the highest frequency (85.5 GHz \approx 3.5 mm) was 4.2×6.8 km (cross-track X along track) with the other bands having lower resolutions decreasing to 36×60 km at (10.6 GHz \approx 3.0 cm) with 13.9 km between successive scans. Since the scaling properties of the horizontal and vertical polarizations were very similar, we only analyzed the five vertically polarized bands indicated in Table 2. Finally, we have included analysis of the active (PR) sensor which is a 2.2 cm wavelength radar with resolution 4.3 km in the horizontal and 250 m in the vertical (only near surface reflectivities were considered).

[7] Although analyses were performed on orbits 538 through 1538 (roughly January and February 1998), each band has differing fractions of missing data (4–15% were discarded). This roughly two month period was chosen because it was about 2–4 times the typical lifetime of global scale structures (the “synoptic maximum”): analysis of first half of the data indeed gave nearly identical results.

3. Analysis

[8] If atmospheric dynamics are controlled by scale invariant turbulent cascades of various (scale by scale) conserved fluxes φ then the fluctuations $\Delta I(\Delta x)$ in the radiances over a distance Δx are related to the turbulent fluxes by a relation of the form $\Delta I(\Delta x) \approx \varphi \Delta x^H$ (this is a generalization of the Kolmogorov law for velocity fluctuations). Without knowing H - nor even the physical nature of the flux - we can use this to estimate the normalized (nondimensional) flux at the smallest resolution of our data: $\varphi/\langle\varphi\rangle = \Delta I/\langle\Delta I\rangle$ (where “ $\langle \rangle$ ” indicates statistical averaging). In this case, $\Delta I(\Delta x)$ was estimated by absolute differences: $\Delta I(\Delta x) = |I(x + \Delta x) - I(x)|$ with Δx the smallest reliable resolution and x an along track coordinate, but other definitions of fluctuations could be used. This flux can then be degraded (by averaging) to a lower resolution L . If the fluxes are realizations of pure multiplicative cascades then the normalized statistical moments M_q obey the generic multiscaling relation:

$$M_q = \left(\frac{\lambda}{\lambda_{eff}} \right)^{K(q)}; \lambda = L_{earth}/L; \lambda_{eff} = L_{earth}/L_{eff} \quad (1)$$

where $M_q = \langle \varphi_\lambda^q \rangle / \langle \varphi_\lambda \rangle^q$ and L_{eff} is the effective outer scale of the cascade. $\langle \varphi_\lambda \rangle$ is the ensemble mean large scale (i.e., the

climatological value). λ is a convenient scale ratio based on the largest great circle distance on the earth $L_{earth} = 20,000$ km and the scale ratio λ/λ_{eff} is the overall ratio from the scale where the cascade started to the resolution scale L , λ_{eff} is determined empirically.

[9] In Figure 1 we show the results on the 5 VIRS bands. For reference, we have plotted the regressions in which the slope $K(q)$ was fitted to each line, and the intercept forced to go through the common point $\lambda = \lambda_{eff}$. We see that to high accuracy out to near planetary scales, the only significant qualitative difference between the flux statistics for different wavelengths is the outer scale. From Table 1 we can see that L_{eff} is in the range of about 11000–28000 km. This cascade “signature” of converging lines shows that the variability of weak and strong structures (large and small q) is the same as that produced by a multiplicative cascade. From the figures we see that the very large scales depart a little from the pure scaling only for scales >5000 km (far left). To further quantify the differences between wavelengths we must compare the slopes (the $K(q)$ functions). A simple way to do this which is valid near the mean ($q = 1$) is to use the parameter $C_1 = K'(1)$ called “the codimension of the mean”; see Table 1. C_1 quantifies the sparseness of the field values which give the dominant contributions to the mean (for a full characterization, universal multifractals can be used [e.g., *Schertzer and Lovejoy, 1987*]).

[10] To understand Table 1, we note that the VIRS bands 1, 2 are essentially reflected sunlight (with very little emission and absorption) so that for thin clouds, the signal comes from variations in the surface albedo (influenced by the topography and other factors), while for thicker clouds it comes from nearer the cloud top via (multiple) geometric and Mie scattering. As the wavelength increases into the thermal IR, the radiances are increasingly due to black body emission and absorption with very little multiple scatter. Whereas at the visible wavelengths we would expect the signal to be influenced by the statistics of cloud liquid water density ($C_1 \approx 0.07$ [*Lovejoy and Schertzer, 1995; Davis et al., 1996*])—itself close to those of passive turbulent scalars ($C_1 \approx 0.04$; see the reviews by *Lovejoy et al. [2008b]*, *Lilley et al. [2008]*, and *Radkevitch et al. [2008]*)—for the thermal IR wavelengths it would rather be dominated by the statistics of temperature variations ($C_1 \approx 0.10$ [*Lilley et al., 2008*])—themselves also close to those of passive scalars. Elsewhere we quantify the shape of the $K(q)$ curves using universal multifractals showing that the $K(q)$ functions are close to those of previous visible and infra red studies performed at smaller scales (ground photography, SPOT, AVHRR and GMS satellites [*Lovejoy and Schertzer, 2006*]).

Table 2. Characteristics of the Five TMI Bands^a

Band	Wavelength	Resolution (km)	$\bar{\delta}$ (%)	C_1	L_{eff} (km)
TMI1	3.0 cm (10.6 GHz)	111.4	1.01	0.255	15900
TMI 3	1.58 cm (19.35 GHz)	55.6	1.25	0.193	6900.
TMI 5	1.43 cm (22.235 GHz)	27.8	1.66	0.157	5000.
TMI 6	8.1 mm (37 GHz)	27.8	1.51	0.15	4400.
TMI 8	3.51 mm (85.5 GHz)	13.9	1.26	0.102	6300.
TRMM ^b Z	2.2 cm (13.2GHz)	4.3	5.9 ^b	0.63	32000

^aAll used vertical polarization.

^bZ = radar reflectivity factor, from *Lovejoy et al. [2008a]*. The minimum detectable signal is twice the mean so that most of the deviations from scaling are at low q .

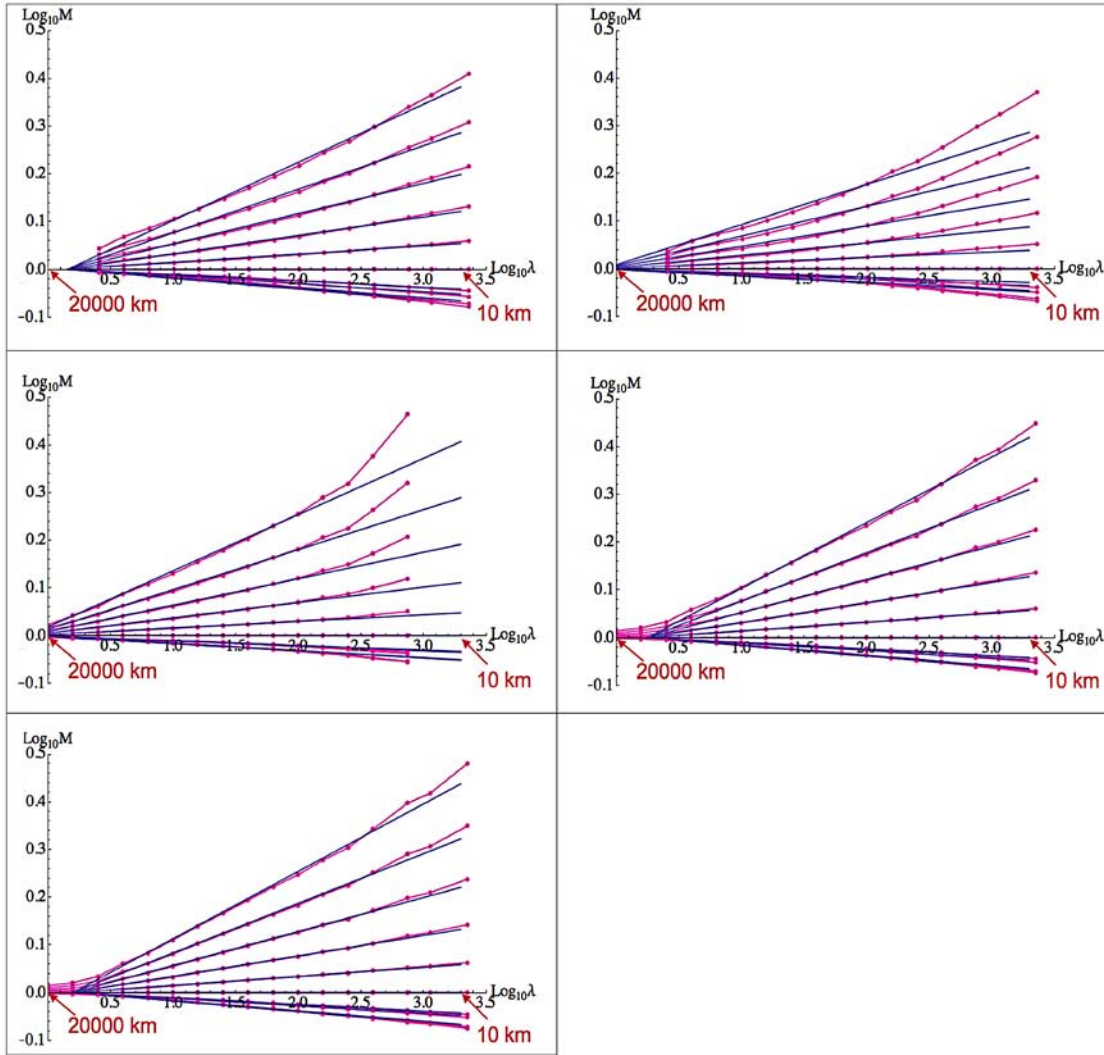


Figure 1. This shows the moments $q = 0.2, 0.4 \dots 1.8, 2.0$, of the cascade fluxes associated with the radiances from VIRS bands 1–5 (left to right, top to bottom); $\lambda = 1$ corresponds to 20000 km. With the exception of the $q < 0.5$ lines, the curves increase with q monotonically from bottom to top. The blue lines are the regressions through the common outer scales indicated in Table 1, for each q , the slopes are the estimates of $K(q)$.

[11] In order to quantify the accuracy to which scaling is obeyed, we can determine the small deviations by estimating the mean absolute residuals:

$$\Delta = \overline{|\log_{10}(M_q) - K(q) \log_{10}(\lambda/\lambda_{eff})|} \quad (2)$$

For each q , Δ is determined from the linear regression on Figure 1; the slopes yield $K(q)$ and λ_{eff} is determined from the intercept (fixed to be the same for all q). The overbar in equation (2) indicates averaging over the different λ (at intervals of $10^{0.2}$) over the available range of scales up to 5000 km. For $0 \leq q \leq 2$ (corresponding to >90% of the data) we find that the scaling of the fluxes is within $\Delta = 0.015$. Defining the percentage deviation $\delta = 100 \times (10^\Delta - 1)$ this implies $\delta < \pm 0.35\%$. The mean δ over the range $0 \leq q \leq 2$ ($\bar{\delta}$) is given in Table 1; it is in the range ± 0.35 to $\pm 0.61\%$.

[12] The analogous analyses for the TMI data are shown in Figure 2 with λ_{eff} , $\bar{\delta}$ given in Table 2. We see that $\bar{\delta}$ is a little larger than for the VIRS ($\pm 1.01\% - \pm 1.66\%$). At the same

time, as the wavelength increases from TMI 8 (≈ 3.5 mm) to TMI 1 (≈ 3.0 cm), C_1 tends to increase from roughly the VIRS value (≈ 0.10) to 0.26. It is instructive to compare these values to those of the TRMM (near surface radar reflectivity (Z ; Figure 3 and bottom line of Table 2). We see that Z has an extremely high C_1 ; it also has stronger variability with L_{eff} somewhat larger than the size of the earth implying that due to interactions with other atmospheric fields even globally averaged Z 's have the same residual variability that they would have had if the cascade had reached 32,000 km. Although a curvature is visible for the low q values, *Lovejoy et al.* [2008a] quantitatively explain this as an artifact of the insensitivity of the radar to low reflectivity values (the corresponding C_1 for the rain rate is ≈ 0.3 , although this depends on the Z – R relation and will be discussed elsewhere). The ability of the model to accurately predict not only the first order behaviour-but also the deviations from that behaviour—lends it further support.

[13] To understand these results, recall that the thermal microwave radiation has contributions from surface reflec-

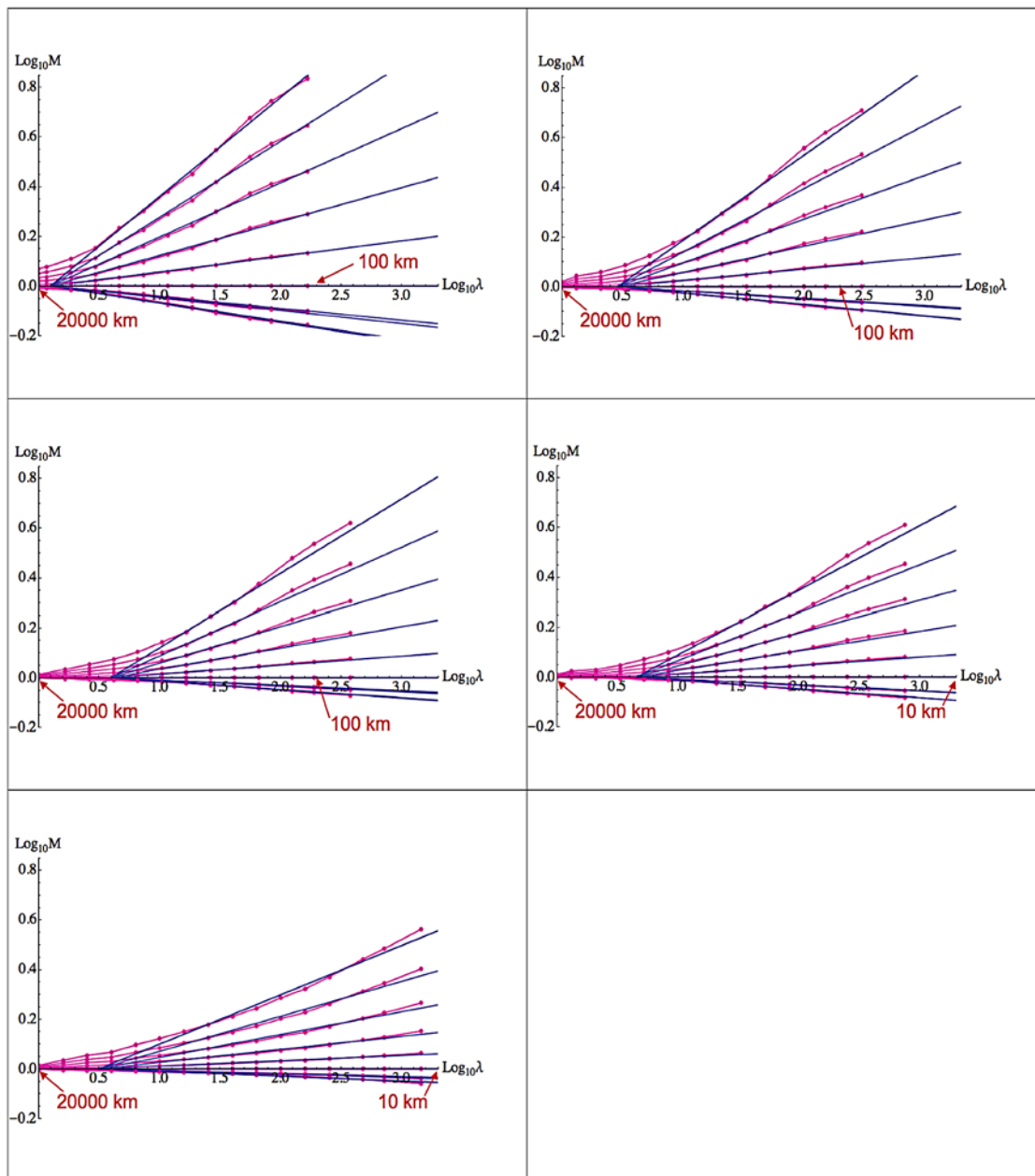


Figure 2. Same as Figure 1 but radiances from TMI bands 1, 3, 5, 6, 8 (left to right, top to bottom). The blue lines are the regressions through the common outer scales indicated in Table 2.

tance, water vapour and cloud and rain. Since the particles are smaller than the wavelengths this is the Rayleigh scattering regime and as the wavelength increases from ≈ 3.5 mm to ≈ 3.0 cm the emissivity/absorptivity due to cloud and precipitation decreases so that more and more of the signal originates in the lower reaches of clouds and underlying surface. Also, the ratio of absorption to scattering decreases so that at 3 cm multiple scattering can be important in raining regions. The overall result is that the horizontal gradients - which we have used to estimate the cascade fluxes - will increasingly reflect large internal liquid water gradients. We therefore expect the longer wavelengths to give flux statistics close to those of the (2.2 cm) radar reflectivity signal (which is proportional to the second moment of the particle vol-

umes). This explanation is consistent with the trend mentioned above for C_1 to increase sharply at the longest wavelengths towards the reflectivity value. The relative similarity of the TMI 1 band and Z (and the other bands with the VIRS) is also supported by the fact that the outer scale is in the 5,000–7,000 km range for the longer wavelengths but is nearly 16,000 km—approaching the reflectivity outer scale—in the TMI 1.

4. Conclusions

[14] It is paradoxical that in spite of growing quantities of atmospheric data that there is still no accepted picture of the scale by scale statistical properties of the atmosphere, yet the high accuracy ($\approx \pm 1\%$) with which we show the cascade

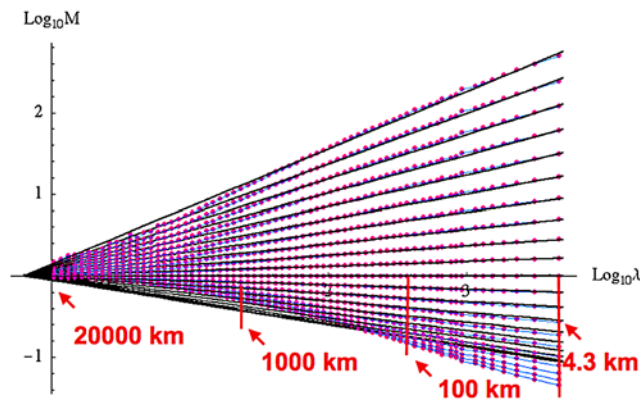


Figure 3. Same as Figure 1 but reflectivities from the precipitation radar (wavelength 2.2 cm), $q = 0.1, 0.2, \dots, 1.9, 2.0$. $\lambda = 1$ corresponds to 20000 km. The black lines are the regressions through the common outer scale indicated in Table 2 [adapted from Lovejoy *et al.*, 2008a].

structure to be respected makes it one of the most accurately obeyed atmospheric laws. Since the radiances are strongly coupled with the dynamics, it is hard to avoid the conclusion that the latter are spatially scaling over virtually the entire meteorologically relevant range. Elsewhere but with important nuances, we show that this conclusion also holds for temporal scaling.

[15] So which Richardson is right? The father of NWP or the grandfather of cascades? The answer may be both. This is possible because cascade models are specifically designed to satisfy many of the basic symmetries of the nonlinear PDE's especially the scaling itself but also the scale by scale conservation of fluxes such as energy which are conserved by the nonlinear terms. Up until now, the scaling (but not directly cascade) properties of the models have been primarily studied in the time domain [Syroka and Toumi, 2001; Blender and Fraedrich, 2003; Fraedrich and Blender, 2003; Kiehl and Trenberth, 1997], however models are now large enough so that their (possible) spatial cascade properties can be directly studied. Analysis on a typical GCM (the Canadian GEM model (J. Stolle *et al.*, The stochastic cascade structure of deterministic numerical models of the atmosphere, *Physica A*, 2008)) do indeed show cascade behaviour in the horizontal wind up to $\approx 10,000$ km, so that the models catch a glimpse of the first factor of ≈ 30 of a cascade which might continue down to millimeter scales. Conventional models therefore already implicitly use cascades; however there are also explicit space-time stochastic cascade models [Marsan *et al.*, 1996; Schertzer and Lovejoy, 2004; S. Lovejoy and D. Schertzer, On the numerical simulation of continuous in scale isotropic universal multifractals, submitted to *Computers and Geoscience*, 2008] which have the advantage of being able take into account arbitrarily large ranges of scale and of being able to directly produce “ensemble” forecasts. Since modern ensemble forecast systems require assumptions about the stochastic structure of the atmosphere, our results have direct applications for conventional modeling (e.g., “stochastic parameterisations” [Palmer, 2001]). Since current earth radiation budgets estimates do not take the implied systematic scale-dependent biases into account, there will also be applications to the assessment of climate change and to remote sensing.

[16] The history of science has shown that apparently complex phenomena usually end up giving way to simplicity, and that simplicity points the way to the future. In this case, the discovery that model dynamics are themselves accurately modeled by cascade processes opens up promising new (stochastic) ways of understanding, modeling and forecasting the atmosphere [Schertzer and Lovejoy, 2004] that directly exploit the scale by scale simplicity allowing us to model the enormous range of scales found in the atmosphere.

[17] **Acknowledgments.** This work was carried out for purely scientific purposes; there was no specific support. S. King acknowledges a McGill undergraduate summer stipend, J. Stolle an NSERC graduate scholarship, T. Bourgeois a summer stipend from the École Nationale des Ponts et Chaussées. We would like to thank the editors of *Science* and of *Nature Geophysics* for finding this report too “specialist,” and to the editors of the *Bulletin of the American Meteorological Society* for finding it “exotic.”

References

- Barnes, R. A., *et al.* (1999), An overview of the visible and infrared scanner radiometric calibration algorithm, *J. Atmos. Oceanic Technol.*, *17*, 395–405.
- Blender, R., and K. Fraedrich (2003), Long time memory in global warming simulations, *Geophys. Res. Lett.*, *30*(14), 1769, doi:10.1029/2003GL017666.
- Boer, G. J., and T. G. Shepherd (1983), Large scale two-dimensional turbulence in the atmosphere, *J. Atmos. Sci.*, *40*, 164–184.
- Chen, T.-C., and A. Wiin-Nielsen (1978), Non-linear cascades of atmospheric energy and enstrophy in a two-dimensional spectral index, *Tellus*, *30*, 225–230.
- Davis, A., *et al.* (1996), Scale invariance of liquid water distributions in marine stratocumulus. Part I: Spectral properties and stationarity issues, *J. Atmos. Sci.*, *53*, 1538–1558.
- Fraedrich, K., and R. Blender (2003), Scaling of atmosphere and ocean temperature correlations in observations and climate models, *Phys. Rev. Lett.*, *90*, 108501, doi:10.1103/PhysRevLett.90.108501.
- Kiehl, J. T., and K. E. Trenberth (1997), Earth's annual global mean energy budget, *Bull. Am. Meteorol. Soc.*, *78*, 197–208.
- Kummerow, C., *et al.* (1997), The Tropical Rainfall Measuring Mission (TRMM) sensor package, *J. Atmos. Oceanic Technol.*, *15*, 809–817.
- Lilley, M., *et al.* (2008), Scaling turbulent atmospheric stratification, part II: Empirical study of the stratification of the intermittency, *Q. J. R. Meteorol. Soc.*, *134*, 317–335, doi:10.1002/qj.1202.
- Lovejoy, S., and D. Schertzer (1995), How bright is the coast of Brittany? in *Fractals in Geoscience and Remote Sensing*, edited by G. Wilkinson, pp. 102–151, Off. for Off. Publ. of the Eur. Comm., Luxembourg.
- Lovejoy, S., and D. Schertzer (2006), Multifractals, cloud radiances and rain, *J. Hydrol.*, *322*, 59–88, doi:10.1016/j.jhydrol.2005.02.042.
- Lovejoy, S., *et al.* (1986), Fractal characterisation of inhomogeneous measuring networks, *Nature*, *319*, 43–44.
- Lovejoy, S., D. Schertzer, and J. D. Stanway (2001), Direct evidence of planetary scale atmospheric cascade dynamics, *Phys. Rev. Lett.*, *86*, 5200–5203.
- Lovejoy, S., *et al.* (2004), Fractal aircraft trajectories and nonclassical turbulent exponents, *Phys. Rev. E*, *70*, 036306, doi:10.1103/PhysRevE.70.036306.
- Lovejoy, S., *et al.* (2008a), The remarkable wide range scaling of TRMM precipitation, *Atmos. Res.*, *90*, 10–32, doi:10.1016/j.atmosres.2008.02.016.
- Lovejoy, S., *et al.* (2008b), Scaling turbulent atmospheric stratification, part I: Turbulence and waves, *Q. J. R. Meteorol. Soc.*, *134*, 277–300, doi:10.1002/qj.1201.
- Mandelbrot, B. B. (1974), Intermittent turbulence in self-similar cascades: Divergence of high moments and dimension of the carrier, *J. Fluid Mech.*, *62*, 331–350.
- Marsan, D., D. Schertzer, and S. Lovejoy (1996), Causal space-time multifractal processes: Predictability and forecasting of rain fields, *J. Geophys. Res.*, *101*(D21), 26,333–26,346.
- Novikov, É. A., and R. Stewart (1964), Intermittency of turbulence and spectrum of fluctuations in energy-dissipation, *Izv. Akad. Nauk. SSSR. Ser. Geofiz.*, *3*, 408–412.
- Palmer, T. (2001), Predicting uncertainty in numerical weather forecasts, in *Meteorology at the Millennium*, edited by R. P. Pearce, pp. 3–13, Academic, San Diego, Calif.
- Radkevitch, A., *et al.* (2008), Scaling turbulent atmospheric stratification,

- part III: Empirical study of space-time stratification of passive scalars using lidar data, *Q. J. R. Meteorol. Soc.*, *134*, 317–335, doi:10.1002/qj.1203.
- Richardson, L. F. (1922), *Weather Prediction by Numerical Process*, Cambridge Univ. Press, New York. (republished by Dover, Mineola, N. Y. 1965.)
- Richardson, L. F. (1926), Atmospheric diffusion shown on a distance-neighbour graph, *Proc. R. Soc., Ser. A*, *110*, 709–737.
- Schertzer, D., and S. Lovejoy (1987), Physical modeling and analysis of rain and clouds by anisotropic scaling of multiplicative processes, *J. Geophys. Res.*, *92*, 9693–9714.
- Schertzer, D., and S. Lovejoy (2004), Uncertainty and predictability in geophysics: chaos and multifractal insights, in *State of the Planet, Frontiers and Challenges in Geophysics*, *Geophys. Monogr. Ser.*, vol. 150, edited by R. S. J. Sparks and C. J. Hawkesworth, pp. 317–334, AGU, Washington, D. C.
- Strauss, D. M., and P. Ditlevsen (1999), Two-dimensional turbulence properties of the ECMWF reanalyses, *Tellus, Ser. A*, *51*, 749–772.
- Syroka, J., and R. Toumi (2001), Scaling and Persistence in Observed and Modeled Surface Temperature, *Geophys. Res. Lett.*, *28*(17), 3255–3258.
- TRMM Precipitation radar team (2005), Tropical Rainfall Measuring Mission, Precipitation Radar Algorithm Instruction Manual for Version 6, Japan Aerospace Exploration Agency (JAXA), National Aeronautics and Space Administration (NASA), 180 pp.
- Yaglom, A. M. (1966), The influence on the fluctuation in energy dissipation on the shape of turbulent characteristics in the inertial interval, *Sov. Phys. Dokl.*, *2*, 26–30.

V. Allaire, S. King, S. Lovejoy, J. Piel, and J. Stolle, Physics, McGill University, 3600 University Street, Montreal, QC H3A 2T8, Canada. (lovejoy@physics.mcgill.ca)

T. Bourgeois and D. Schertzer, CERERE, Université Paris Est, F-77455 Marnella-Vallée, France. (daniel.schertzer@cereve.enpc.fr)